SCHMID, M. F., WEAVER, L. H., HOLMES, M. A., GRÜTTER, M. G., OHLENDORF, D. H., REYNOLDS, R. A., REMINGTON, S. J. & MATTHEWS, B. W. (1981). *Acta Cryst.* A37, 701–710.
SILVA, A. M. & ROSSMANN, M. G. (1987). *J. Mol. Biol.* **197**, 69–87.
STEIGEMANN, W. (1974). PhD Thesis, Technische Univ., München, Germany.
TOLLIN, P. & ROSSMANN, M. G. (1966). *Acta Cryst.* **21**, 872–876.
VALEGÅRD, K., LILJAS, L., FRIDBORG, K. & UNGE, T. (1990). *Nature (London)*, **345**, 36–41.
VALEGÅRD, K., UNGE, T., MONTELIUS, I., STRANDBERG, B. & FIERS, W. (1986). *J. Mol. Biol.* **190**, 587–591.
WINKLER, F. K., SCHUTT, C. E. & HARRISON, S. C. (1979). *Acta Cryst.* A35, 901–911.

Acta Cryst. (1991). B47, 960–968

The Variety of X-ray Diffuse Scattering from Macromolecular Crystals and its Respective Components

BY I. D. GLOVER

Department of Physics, University of Keele, Keele, Staffordshire ST5 5BG, England, and SERC Daresbury Laboratory, Daresbury, Cheshire WA4 4AD, England

G. W. HARRIS*

Department of Crystallography, Birkbeck College, Malet Street, London WC1E 7HX, England

J. R. HELLIWELL

Department of Chemistry, University of Manchester, Manchester M13 9PL, England, and SERC Daresbury Laboratory, Daresbury, Cheshire WA4 4AD, England

AND D. S. MOSS

Department of Crystallography, Birkbeck College, Malet Street, London WC1E 7HX, England

(*Received* 30 *November* 1989; *accepted* 16 *April* 1991)

Abstract

A range of protein single-crystal diffraction patterns, recorded with intense collimated synchrotron X-radiation are presented. These patterns illustrate the rich and varied nature of the diffuse scattering from this kind of crystal and suggest that the continuous background diffraction will be a source of specific information on the molecular dynamics and flexibility of particular proteins. The relative contributions of the background X-ray diffuse scattering from the solvent, the glass capillary and the sample have been quantified for two of the samples; the so-called solvent ring is shown to be due principally to protein disorder in the crystal both because of the intensity and the marked anisotropy of the ring in specific cases. The form of the acoustic scattering associated with the Bragg peaks was studied in ribonuclease, and is shown, at low resolution at least, to be explained in terms of single-phonon interactions.

* Present address: AFRC Institute of Food Research, Shinfield, Reading, Berkshire RG2 9AT, England.

1. Introduction

A characteristic feature of protein crystals is that their diffraction patterns often extend to limited resolutions. This feature is particularly apparent in medium to large proteins where diffraction data often do not reach 2 Å resolution. This restricted quantity of Bragg data becomes a limiting factor when studying conformational flexibility and it is precisely those proteins where flexibility is likely to be most important which yield fewest Bragg data and exhibit the strongest diffuse scattering.

The diffuse background on an X-ray diffraction pattern may arise from several sources including thermal diffuse scattering, static disorder, solvent disorder, Compton scattering, fluorescence, scattering from mounting tubes, air scattering and the intrinsic film fog. The static or dynamic displacement of atoms in a crystal may be due to a variety of causes, such as the optic and acoustic modes of vibration within the crystal, diffusional motion on the surface of macromolecules (dynamic), or positional and orientational disorder (static) within mol-

0108-7681/91/060960-09$03.00

ecules. Such disorder causes a breakdown in the crystal translational symmetry and a reduction in Bragg intensities at high resolution and the concommitant appearance of diffuse scattering at and between the reciprocal lattice points. In macromolecular crystals the diffuse scattering is often quite strong, rich in detail and apparently quite peculiar to the crystal form, and represents a potentially rich source of information regarding atomic displacements.

In the case of static disorder unit cells exist with different arrangements of the time-averged atomic positions. Orientational disorder occurs in molecular crystals where molecules, flexible side groups or domains may take up different positions, breaking down translational symmetry. Dynamic disorder in macromolecular crystals may be of many kinds. Diffusional motion of surface side chains, torsional librations of buried groups, relative motions of structural domains ('hinge bending') and local denaturation occurring on time scales from 10^{-11} to 1 s are examples of anharmonic motions which will generally exhibit no long-range correlations in the crystal structure. In addition, two types of lattice vibration may be distinguished, acoustic modes due to ultrasonic waves propagating in the crystal and optic modes of vibration such as those observed in infrared and Raman spectra. Ultrasonic (acoustic) vibrations, occurring on time scales ranging from 10^{-6} to 10^{-10} s, give rise to diffuse scattering which peaks at the reciprocal lattice positions and is observed characteristically as haloes around the Bragg peak. Optic mode vibrations, along with most other types of dynamic and static disorder, give rise to diffuse scattering which is distributed continuously but non-uniformly throughout reciprocal space and is often observed as lines or streaks in a diffraction pattern and is often strongly oriented.

From the experimental viewpoint all types of diffuse scattering will be present in a diffraction pattern from a molecular crystal. The effects will be due to a variety of factors but it is usually not possible to distinguish between them on the basis of the X-ray photograph alone.

In this paper we illustrate the rich and varied nature of the molecular diffuse-scattering patterns from macromolecular crystals recorded with synchrotron radiation. We examine its distribution through scattering angle and show that the commonly observed 'solvent ring' is a misnomer being composed of a radially symmetric solvent contribution and a strong non-symmetric 'molecular' diffuse-scattering component extending to lower resolutions. The form of the acoustic scattering is also discussed and compared with theoretical formulations and the inelastic scattering events giving rise to it.

This paper is divided into three parts. Firstly, we give our observations on a variety of systems selected from many that have been studied at the Daresbury synchrotron radiation source (SRS) or that other workers have brought to our attention from other synchrotron facilities. Secondly, we detail the different contributing components to the 'diffuse-diffraction ring' and compare the experimental results with the theory for an ideal solid. Thirdly, we examine the experimental form of the acoustic scattering for one example and compare it with theoretical predictions. Synchrotron radiation was needed because of its high intensity and collimation. This allowed the relatively weak background scatter to be recorded with sufficient intensity whilst allowing the immediate vicinity of a Bragg peak and any diffuse shoulder to be investigated. Although monochromatic data-collection methods have been used in all cases, white-beam Laue-diffraction methods may, however, be useful in investigating the nature of diffuse-scattering features (M. M. Harding, personal communication).

2. Diversity of the observed diffuse scattering

2.1. *Experimental details*

A series of oscillation and stationary crystal diffraction patterns have been recorded from a variety of protein crystal samples all exploiting the high intensity and small beam divergences of synchrotron radiation beamlines at the SRS (Daresbury), DESY (Hamburg) and SSRL (Stanford). The size and diffracting power of the crystals varies widely as do the observed diffuse-scattering features. The diffraction patterns from avian pancreatic polypeptide (aPP) were recorded at DESY, Hamburg. Bovine ribonuclease A (RNAse), glutamate dehydrogenase (GDH) (the latter courtesy of D. Rice, Sheffield University), rabbit serum transferrin, avian γII-crystallin and 6-phosphogluconate dehydrogenase (6PGDH) have all been examined at the SRS. The diffraction patterns of t-RNA(Met) were supplied by P. Sigler, University of Chicago, and were recorded at SSRL, Stanford. The recorded diffraction pattens are shown in Figs. 1 and 2. The diffuse-scattering features were apparently independent of radiation damage to the crystals.

2.2. *Examples of diffuse scattering from macromolecular crystals*

aPP. Space group $C2$, $a = 34{\cdot}18$, $b = 32{\cdot}92$, $c = 28{\cdot}45$ Å, $\beta = 105{\cdot}3^{\circ}$ (Wood, Pitts, Blundell & Jenkins, 1977). aPP is a small 36-residue polypeptide hormone; the crystals have a low solvent content and diffract to extremely high resolution ($< 0{\cdot}98$ Å using conventional sources). The diffraction patterns show

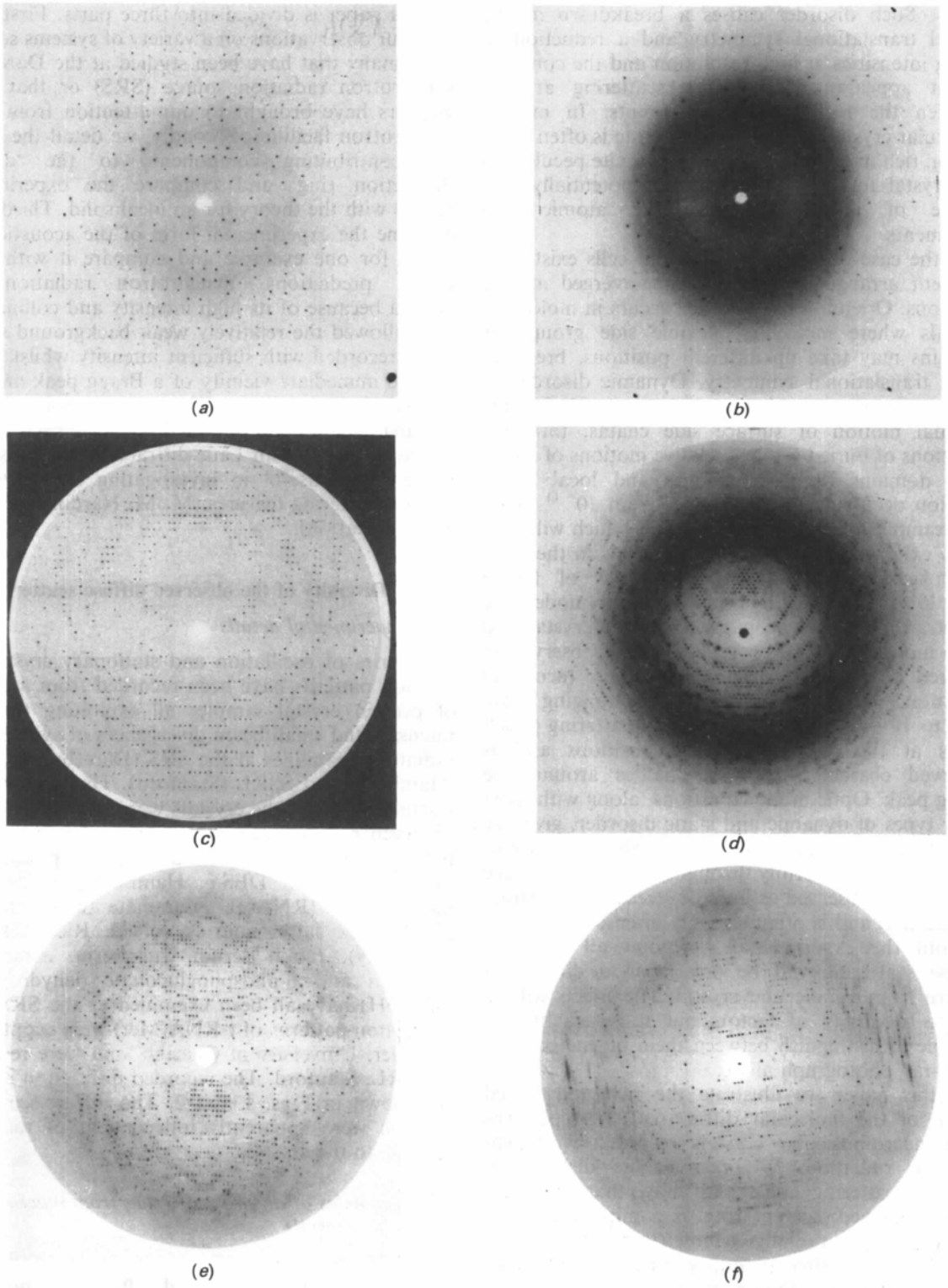

Fig. 1. Single-crystal diffraction patterns recorded from a variety of macromolecular crystals illustrating the variety of diffuse-scattering features. (*a*) aPP, resolution limit 1·8 Å wavelength 1·49 Å, 4·9° oscillation photograph. (*b*) RNAse, resolution limit 1·9 Å, wavelength 1·488 Å, still exposure. (*c*) 6-PGDH with bound 2′-AMP, 1·4° oscillation photograph, incident wavelength 1·488 Å, resolution limit 2·8 Å. (*d*) GDH, 1·5° oscillation photograph, resolution limit 1·9 Å. (*e*) Transferrin, 1·0° oscillation photograph, resolution limit 3·3 Å, incident wavelength 1·74 Å. (*f*) t-RNA(met) 1·5° oscillation pattern, wavelength 1·54 Å.

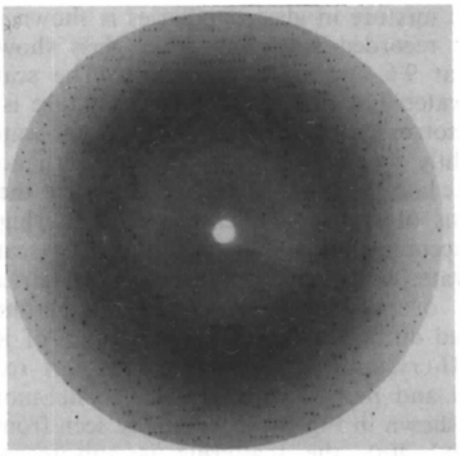

(*a*)

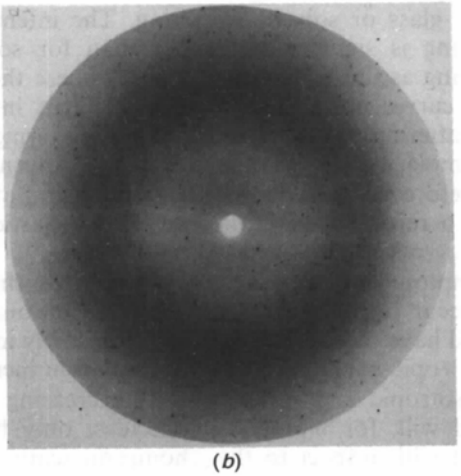

(*b*)

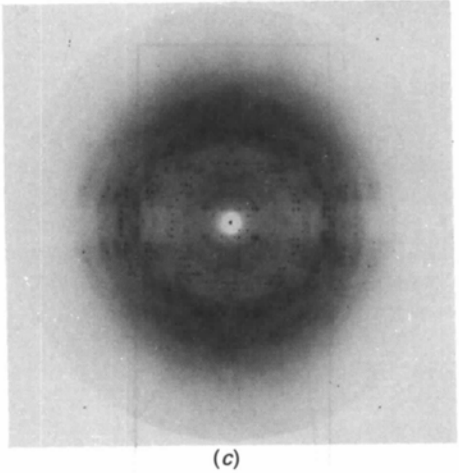

(*c*)

Fig. 2. Still diffraction patterns recorded from native and modified crystals of γII-crystallin. (*a*) Native crystal. (*b*) Crosslinked crystal (2·5% gluteraldehyde). Resolution limit approximately 2·25 Å with noticeable diffuse scattering. (*c*) Crosslinked crystal soaked in 10 n*M* thiomersal. Resolution limit 2·8 Å with a drastic increase in diffuse scattering. All patterns were recorded at SRS, Daresbury, incident wavelength 1·488 Å, with identical crystal-to-film distances and exposure times.

very little background diffuse scattering and little indication of acoustic scattering. It is somewhat uncharacteristic of a macromolecular crystal with most scattered radiation appearing as elastically scattered Bragg reflections and could be termed a 'hard' crystal.

RNAse. Space group $P21$, $a = 30{\cdot}45$, $b = 38{\cdot}37$, $c = 53{\cdot}22$ Å, $\beta = 106°$ (Carlisle, Palmer, Mazumdar, Gorinsky & Yeates, 1974). RNAse is a 10 000 molecular weight enzyme, crystals of which diffract to 1·2 Å using synchrotron radiation. The diffraction pattern shows distinct acoustic diffuse-scattering haloes around many of the Bragg peaks but with little background diffuse scattering observed except for indistinct patches at resolutions above 3·2 Å. The 'solvent' ring is markedly anisotropic and shows considerable inhomogeneity.

6-PGDH and GDH. 6-PGDH, space group $C222_1$ $a = 72{\cdot}72$, $b = 148{\cdot}15$, $c = 102{\cdot}91$ Å (Adams, Helliwell & Bugg, 1977), and GDH, space group $C2$, $a = 147$, $b = 151$, $c = 108$ Å, $\beta = 106°$ (Rice, Hornby & Engel, 1985) are medium to large proteins of molecular weight approximately 50 000 which show features of both acoustic and continuous diffuse scattering. Some evidence of preferential orientation in the continuous diffuse scattering is seen. The diffuse 'solvent' ring is evident and noticeably anisotropic particularly in the case of GDH where it has the form of an approximate pentagon extending from 4·5 to 2·7 Å resolution.

Transferrin. Space group $P4_32_12$, $a = b = 127{\cdot}4$, $c = 145{\cdot}4$ Å (Al-Hilal *et al.*, 1976), molecular weight 80 000. Crystals of transferrin diffract to only about 3 Å but show considerable diffuse scattering seen as a series of streaks running at approximately 45° to the Bragg layer lines. These features are strongest between 5·4 and 3·3 Å resolution. The diffuse-scattering ring builds up at high resolution but the inner (low-resolution) edges form a distinct diamond shape following the orientation of the diffuse-scattering streaks. Chevrons of diffuse scattering, not associated with the layer lines, are seen along the meridian as the limit of the Bragg diffraction is reached.

t-RNA(Met). Space group $P6_422$, $a = b = 113{\cdot}7$, $c = 136{\cdot}25$ Å (courtesy of P. Sigler). The diffraction pattern obtained from the crystals of t-RNA(Met) shows very pronounced diffuse scattering. In the pattern shown, a 1·5° oscillation photograph, the c^* axis is inclined approximately 10° to the horizontal. Equatorially oriented strong diffuse streaks can be seen which are approximately 8 mm long and follow the Bragg layer lines. Further streaking occurs perpendicular to these features again following the layer lines. The strongest diffuse features occur at around 3·3 Å resolution. The diffuse ring peaks at approximately 3·45 Å resolution and forms a diamond

shape. Chevrons of diffuse scattering occur at the extremes of the Bragg diffraction, these features do not follow the layer lines and hence are solely a function of the molecular transform and not the lattice.

γII-*Crystallin*. Space group $P4_12_12$, $a = b = 58{\cdot}1$, $c = 98{\cdot}4$ Å (Carlisle, Lindley, Moss & Slingsby, 1977), molecular weight 20 000. Crystals of the native protein, a principal eye-lens protein, diffract to 1·4 Å on a synchrotron radiation source, but the diffraction patterns shown here (Fig. 2) were recorded to only 2·25 Å resolution and show distinct acoustic scattering but little evidence of oriented diffuse scattering apart from the diffuse ring. Routine crosslinking of the crystals (using 2.5% gluteraldehyde), making them physically more robust before addition of heavy atoms, gives isomorphous crystals from which the Bragg resolution limit is degraded, and the diffuse scattering significantly increases. Further chemical modification of the crystals, *i.e.* the preparation of heavy-atom derivatives, drastically alters the complete diffraction pattern. Fig. 2 shows the severe reduction in Bragg resolution of the diffraction pattern and the concommitant rise and great wealth of detail in the diffuse-scattering component of the total diffraction pattern.

2.3. *Summary of observations*

In the cases cited above the diffuse-scattering features vary widely from crystal to crystal with a common feature of strong diffuse scattering close to the 'solvent' ring. Continuous diffuse-scattering features vary from being almost absent in the case of aPP to the very rich and dominating scattering seen from crystals of t-RNA(Met). Chemical modification drastically alters the appearance of the diffraction pattern degrading the Bragg component and enhancing the diffuse component. The precise mechanism of this change is not clear but the crosslinking and heavy-atom reagents are likely to have an effect on the degree of both the dynamic and substitutional disorder in the crystal and hence cause a breakdown of the lattice sampling.

3. Contributions to the 'diffuse-diffraction ring'

3.1. *Experimental observations*

A common feature of all the diffraction patterns is the presence of an anisotropic ring of inhomogeneous diffuse intensity in the regions between 4·5 and 2·8 Å resolution. These features are clearly not due to solvent scattering alone, either within the crystal or surrounding it, owing to the intensity and marked anisotropy of the observed features. The scattering of a glass capillary (commonly used for mounting crystals) as well as water and a water/ethanol mixture in glass capillaries is shown in Fig. 3. The recorded scattering from glass shows two peaks at 9·6 and 4·1 Å resolution. The scattering from water and the water/ethanol mixture is made up of isotropic rings, peaking at 3·0 Å for water and at slightly lower resolution for water/ethanol, but with the latter showing some broadening of the peak. In terms of scattered intensity the scattering from glass accounts for only 15–20% of the scattering from water or water/ethanol in glass capillaries.

The overall envelope of the experimentally observed diffuse scattering from samples of RNAse and γII-crystallin (see Figs. 1*b* and 2*a*) recorded parallel and perpendicular to the crystal-mounting axis is shown in Fig. 4(*a*). As can be seen from Figs. 1(*d*) and 4(*a*), the scattering is anisotropic and inhomogeneous, peaking at resolutions outside those due to glass or solvent scattering. The intensity of scattering is significantly higher than for solvent scattering as illustrated by Fig. 4(*b*), where the scattering curves are scaled to equal incident intensity and scattering volume. The observed scattering from macromolecular crystal samples in the 'solvent ring' is therefore not principally due to solvent scattering but is a result of static disorder and inelastic scattering events in the crystal.

Compton scattering, or incoherent scattering will also occur under the experimental conditions used but will have the effect of producing a slowly increasing isotropic background as the resolution increases. This isotropic and monotonically increasing background will, for biological molecules, only be significant with respect to the Thompson scattering at higher (< 2 Å) resolutions.

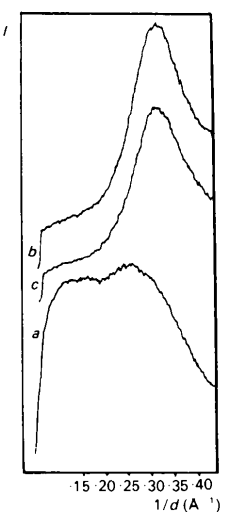

Fig. 3. Densitometered profile from a diffraction pattern recorded with (*a*) a glass crystal-mounting tube. (*b*) Profile from a mounting tube filled with double distilled water. (*c*) Profile from a mounting tube filled with a double distilled water/ethanol mixture [60/40(*v*/*v*)].

3.2. *Theory*

The simplest model of thermal diffuse scattering is one where the crystal is considered to be an Einstein crystal. In this approximation all atoms are assumed to be vibrating independently as harmonic oscillators, each atom having the same mean-squared displacement U. For this model the thermal diffuse scattering is given by:

$$\sum_j f_j^2[1 - \exp(-Q^2U)]$$

where $Q = 4\pi\sin\theta/\lambda$. This is plotted in Fig. 5.

It can be seen that the predicted diffuse scattering peaks between 4 and 5 Å, dependent on the value of U, followed by a gradual fall off as Q increases. Also, it can be seen from Fig. 4(*a*) that the observed diffuse scattering from both RNAse and γII-crystallin does peak, but at about 3·5 Å resolution, and decreases more rapidly than is predicted for an ideal crystal. In particular the diffuse scattering does not appear to increase relative to the Bragg scattering at resolutions higher than 2·5 Å. This last observation is common to most of the samples investigated here with the exception of the t-RNA crystal where the diffuse scattering clearly dominates at high resolution. Thus with t-RNA as a possible exception, a protein crystal is a poor approximation to an ideal solid and correlated motion in addition to static disorder forms a significant contribution to the total observed diffuse scattering.

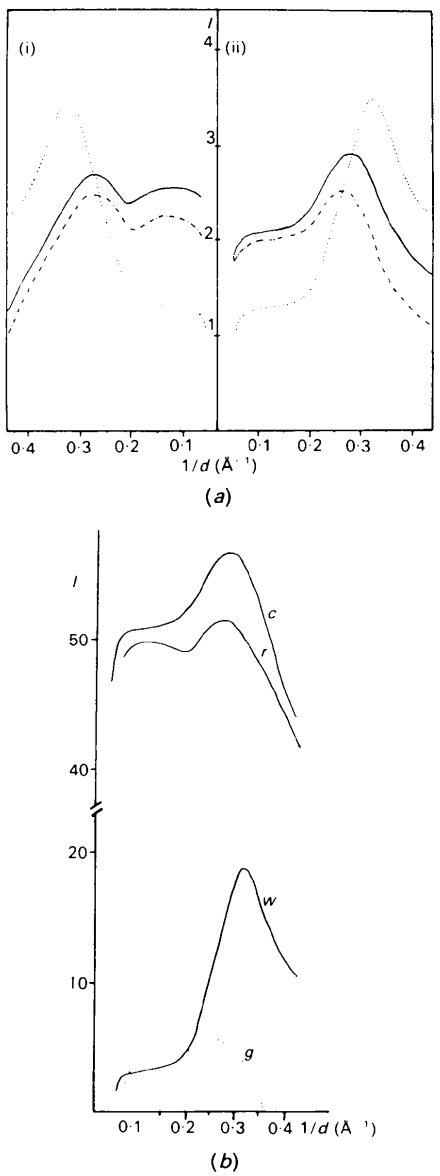

Fig. 4. (*a*) Densitometered profiles from the recorded diffraction patterns of (i) RNAse and (ii) γII-crystallin showing the overall envelope of the observed diffuse scattering intensity (I) recorded parallel (—) and perpendicular (– – –) to the crystal mounting axis. The scattering from water (····) is plotted for comparison. (*b*) The recorded scattering intensity (I) for water (w), RNAse (r) and γII-crystallin (c) scaled to equal scattering volume and incident X-ray intensity curve. Glass scattering (g) is shown for reference.

4. Acoustic scattering

4.1. *Experimental*

The form of the acoustic scattering was investigated using samples of bovine ribonuclease A. The crystals (dimensions 0·5 × 0·5 × 0·5 mm³) were mounted in a capillary in contact with a small drop of the crystal mother liquor (60% water, 40% ethanol). Diffraction patterns were recorded on film using a stationary crystal (*i.e.* *a* still) with exposure times of the order of 20 min (compared to 20 s

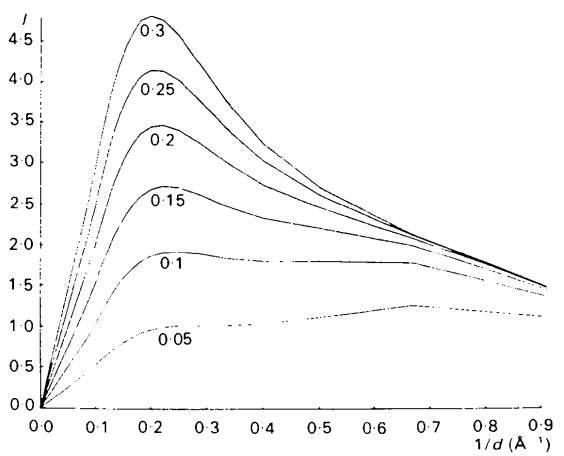

Fig. 5. The overall form for the intensity of diffuse scattering (I) from an ideal solid, calculated for different values of the mean-square displacement U (Å²).

typically required for a normal still) using a bending-magnet beamline at the Daresbury SRS, wavelength 1·488 Å (Nave *et al.*, 1985). A collimator of 0·2 mm diameter was used along with slitting down of the beam premonochromator to reduce further the horizontal beam divergence. Under these conditions the observed Bragg reflection spatial and angular widths are reduced, allowing investigation of the form of the acoustic diffuse-scattering haloes at the reciprocal lattice positions.

Regions of the film containing reflections were densitometered using a Joyce–Loebl flat-bed scanner with a $10 \times 10\ \mu m^2$ raster. Optical density ranges were chosen to show contrast in the diffuse-scattering region leading to saturation in the Bragg peak optical densities. Portions of the film at varying scattering angles were densitometered. Fig. 6 shows the contoured optical density at neighbouring reciprocal lattice positions and line sections through the peaks. The plots clearly show broad diffuse-scattering shoulders to the Bragg peaks, the form of which varies with resolution. At low resolution the shoulders spread least and peak most strongly, the converse being true at higher resolution, indicative of different acoustic scattering (phonon) processes involved in the production of diffuse scattering.

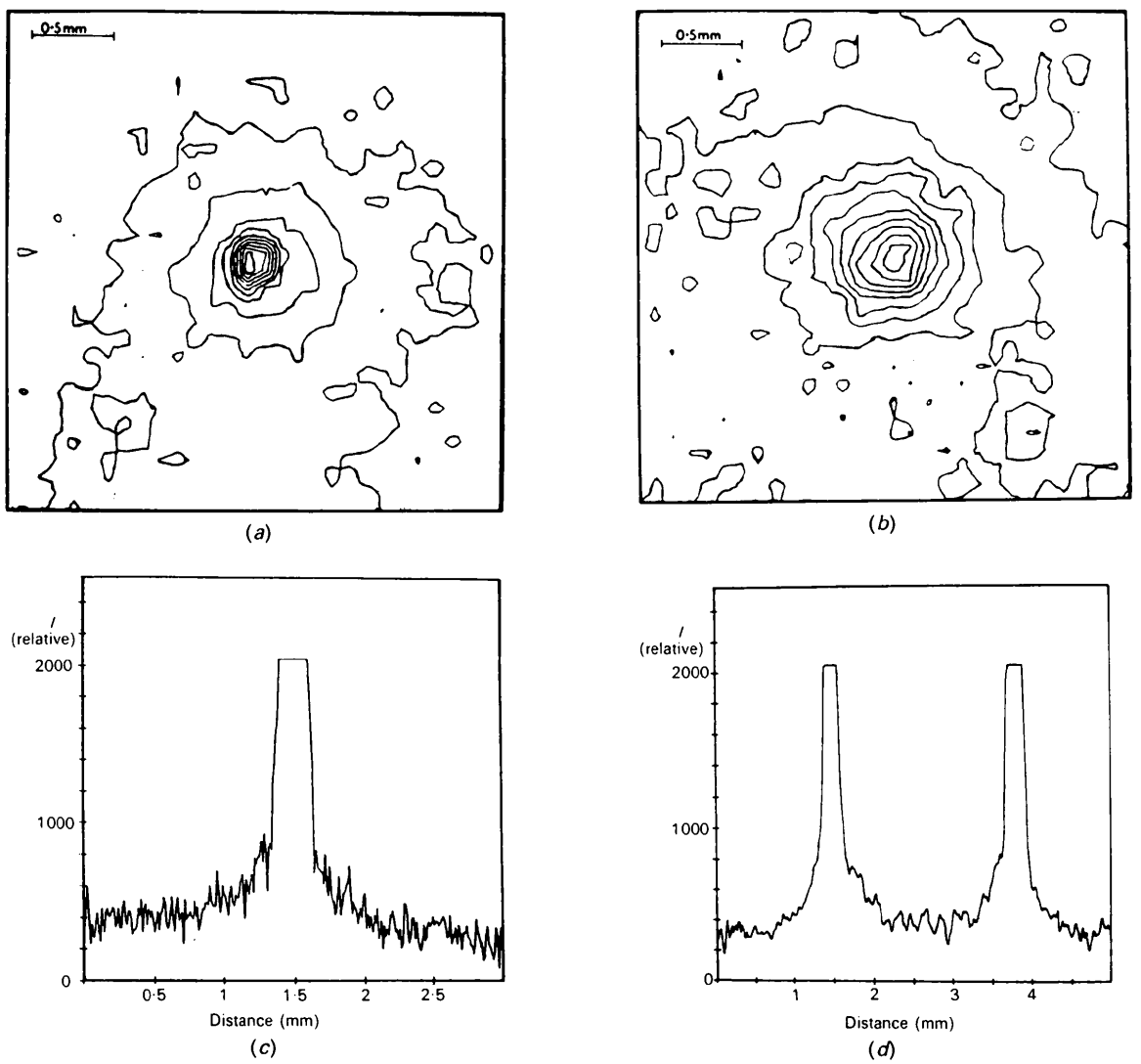

Fig. 6. The form and distribution of acoustic scattering from a crystal of RNAse. $3 \times 3\ mm^2$ boxes contoured according to scattered intensity in the region of (*a*) a low (6 Å) and (*b*) a high (2·8 Å) resolution reflection, both densitometered using a $10 \times 10\ \mu m^2$ raster, and (*c*) and (*d*) line sections through single and adjacent low-resolution Bragg reflections showing clearly resolved but truncated Bragg peaks superimposed upon a broader shoulder of acoustic diffuse scattering.

4.2. *Theory*

The intensity of acoustic diffuse scattering can be described in terms of the phonon (lattice-wave) scattering factors (Moss & Harris, 1991). From the one-phonon structure factor the diffuse-scattered intensity, $I^{(1)}$ is given by:

$$I^{(1)}(\mathbf{Q}) = k_B T \sum_j |G_j^{(1)}(\mathbf{Q})|^2 H(\omega_1)$$

where

$$G^{(1)}(\mathbf{Q}) = \sum_j g_j m_j^{-1/2} (\mathbf{Q}.\mathbf{l}_{ij}) \exp(i\mathbf{Q}.\mathbf{x}_j)$$

and

$$H(\omega_i) = \omega_i^{-2} \Delta(\mathbf{Q} + \mathbf{q}_i).$$

The one-phonon structure contains a vector product $(\mathbf{Q}.\mathbf{l}_{ij})$ of the atomic displacements $\mathbf{l}_{ij}$ with the scattering vector and predicts that the diffuse scattering will be greatest when displacements are parallel to the scattering vector.

The term $H(\omega_i)$ shows the frequency (ω) dependence of one-phonon scattering and predicts that the diffuse scattering will peak at $\mathbf{Q} + \mathbf{q} = 2\pi h$, *i.e.* at the reciprocal lattice position and that $I^{(1)}$ is proportional to $1/\omega^2$, *i.e.* close to the Bragg peak the acoustic diffuse-scattering should fall off as $1/q^2$.

For the two-phonon case

$$I^{(2)}(\mathbf{Q}) = \tfrac{1}{2} k_B^2 T^2 \sum_h \sum_i |G_{hi}^{(2)}(\mathbf{Q})|^2 H(\omega_h \omega_i)$$

where

$$G_{hi}^{(2)}(\mathbf{Q}) = \sum_{\mathbf{j}} g_j m_j^{-1} (\mathbf{Q}.\mathbf{l}_{hj})(\mathbf{Q}.\mathbf{l}_{ij}) \exp(i\mathbf{Q}.\mathbf{x}_j).$$

The terms are similar to the one-phonon case but describe the interaction of the X-ray beam with two-phonon vibrations (h,i) in the crystal and the diffraction effects are found by summing in all vectors in the Brillouin zone. The frequency dependence becomes

$$H(\omega_h \omega_i) = \omega_h^{-2} \omega_i^{-2} \Delta(\mathbf{Q} + \mathbf{q}_h + \mathbf{q}_i)$$

and implies that the intensity varies more slowly than $1/q^2$ in the vicinity of a reciprocal lattice position. These expressions may be generalized to include the effects of higher phonon interactions.

4.3. *Interpretation*

The experimental plot obtained from a low-resolution (6 Å) reflection compared with that calculated for a single-phonon interaction in the crystal is shown in Fig. 7. The close agreement in the overall form of the acoustic scattering with the theoretical curve shows a $1/q^2$ dependence indicating that at low resolution at least the acoustic scattering may be explained in terms of single-phonon interactions. The experimental plot, however, is clearly not smooth, with structure visible due to the form of the one-phonon structure factor. For indexed reflections the form of one-phonon structure factor may hence be derived. At progressively higher resolutions the one-phonon interaction is likely to be less well adhered to, particularly with regard to the experimental plots obtained, and higher order phonon interactions may have to be considered.

5. Discussion

From even the limited number of patterns presented here it is clear that the diffuse-scattering patterns observed from a macromolecular crystals are very rich in detail and in many cases constitute a significant contribution to the total diffraction pattern. Also the distribution of diffuse scattering is clearly not uniform in reciprocal space and differs from one macromolecule to another. In particular, strongly oriented streaks are often seen and the misnamed solvent ring is a region of strong diffuse scattering which is often markedly anisotropic and may contribute more diffracted energy than due to the solvent itself.

Our observations suggest that the continuous diffuse scattering is a potentially rich source of unique dynamic information regarding correlated

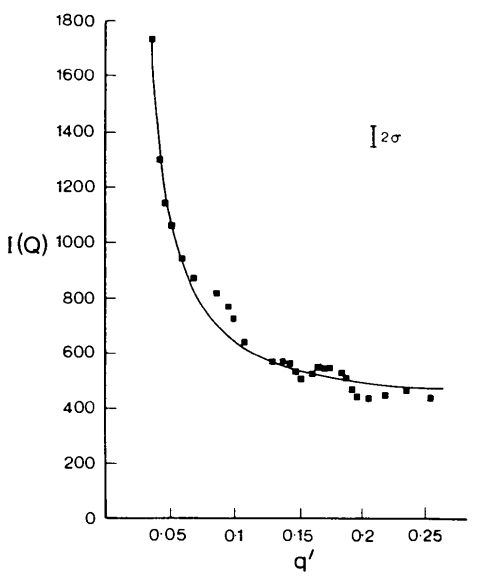

Fig. 7. The observed acoustic diffuse scattering from a 6 Å resolution reflection from ribonuclease superimposed upon the theoretical $1/q^2$ dependence for a single-phonon interaction in the crystal. The overall agreement is good although structure is seen in the observed scattering. The temporal coherence length in the crystal sets an upper limit to the intensity of the predicted diffuse scattering. q' is the fraction of a reciprocal lattice vector between a particular reciprocal lattice point and its neighbour.

atomic displacements in a crystal. Qualitative interpretations of the continuous diffuse scattering in terms of waves of displacement propagating along molecular filaments in tropomyosin (Boylan & Phillips, 1986), correlated rigid-body displacements in lysosyme (Doucet & Benoit, 1987), and atomic displacements and range of coupling in insulin (Caspar, Clarage, Salunke & Clarage, 1988) have been put forward previously. We have developed a more general quantitative approach to the refinement of correlated inter- and intramolecular displacements from diffuse-scattered intensities of molecular crystals (Moss & Harris, 1991). An estimate of the thermal vibration mean-square amplitudes for typical protein crystals has been made using estimates of the longitudinal speed of sound from laser-generated ultrasound measurements and of the transverse speed from Youngs modulus estimates (Edwards *et al.*, 1990).

The acoustic diffuse scattering peaks at the Bragg positions and many constitute a significant source of errors in the integrated intensity measurements. We have exploited the characteristic fine collimation of synchrotron radiation in the collection of data in which the acoustic scattering contributions are minimized to assess the effect on model refinement (I. D. Glover, D. S. Moss, J. R. Helliwell and coworkers, in preparation) and data that allow the modelling of the acoustic diffuse scattering. We have shown that at low resolutions at least the scattering may be explained in terms of one-phonon interactions and that, in principle, the form of the phonon-scattering factors may be extracted from these measurements.

We are grateful to the Science and Engineering Research Council, Birkbeck College and the Universities of Keele, York and Manchester for the support of this work, the Director and Staff at the SERC Daresbury Laboratory for the provision of synchrotron radiation, and to Professor P. Sigler, Dr D. Rice and Dr M. Adams for the provision of experimental data relating to t-RNA(Met), GDH and 6-PGDH respectively.

References

ADAMS, M. J., HELLIWELL, J. R. & BUGG, C. E. (1977). *J. Mol. Biol.* **112**, 183–197.
AL-HILAL, D., BAKER, E., CARLISLE, C. H., GORINSKY, B. A., HORSBURGH, R. C., LINDLEY, P. F., MOSS, D. S., SCHNEIDER, H. & STIMPSON, R. (1976). *J. Mol. Biol.* **108**, 255–257.
BOYLAN, D. & PHILLIPS, G. N. JR (1986). *Biophys. J.* **49**, 76–78.
CARLISLE, C. H., LINDLEY, P. F., MOSS, D. S. & SLINGSBY, C. (1977). *J. Mol. Biol.* **110**, 417–419.
CARLISLE, C. H., PALMER, R. A., MAZUMDAR, S. I., GORINSKY, B. A. & YEATES, D. G. R. (1974). *J. Mol. Biol.* **85**, 1–18.
CASPAR, D. L. D., CLARAGE, J., SALUNKE, D. M. & CLARAGE, M. (1988). *Nature (London)*, **352**, 659–662.
DOUCET, J. & BENOIT, J. P. (1987). *Nature (London)*, **325**, 643–646.
EDWARDS, C., PALMER, S. B., EMSLEY, P., HELLIWELL, J. R., GLOVER I. D., HARRIS, G. W. & MOSS, D. S. (1990). *Acta Cryst.* A**46**, 315–320.
MOSS, D. S. & HARRIS, G. W. (1991). *Acta Cryst.* In preparation
NAVE, C., HELLIWELL, J. R., MOORE, P. R., THOMPSON, A. W., WORGAN, J. S., GREENALL, R. J., MILLER, A., BENTLEY, S. K., BRADSHAW, J., PIGRAM, W. J., FULLER, W., SIDDONS, D. P., DEUTSH, M. & TREGEAR, R. T. (1985). *J. Appl. Cryst.* **18**, 396–401.
RICE, D. W., HORNBY, D. P. & ENGEL, P. C. (1985). *J. Mol. Biol.* **181**, 147–149.
WOOD, S. P., PITTS, J. E., BLUNDELL, T. L. & JENKINS, J. A. (1977). *Eur. J. Biochem.* **78**, 119–126.

Acta Cryst. (1991). B**47**, 968–975

Disordered Fatty-Acid Chains in Piperazinium Myristate and Palmitate

BY L. VENKATRAMANI AND B. M. CRAVEN

Department of Crystallography, University of Pittsburgh, Pittsburgh, PA 15260, *USA*

(*Received* 1 *February* 1991; *accepted* 18 *June* 1991)

Abstract

(I) Piperazinium *n*-tetradecanoate (myristate), $C_4H_{12}N_2^{2+}.2C_{14}H_{27}O_2^-$, $M_r = 542{\cdot}85$, m.p. = 368·9 K, triclinic, $P\bar{1}$, $a = 5{\cdot}681\ (1)$, $b = 7{\cdot}454\ (1)$, $c = 20{\cdot}676\ (3)$ Å, $\alpha = 84{\cdot}59\ (1)$, $\beta = 86{\cdot}37\ (1)$, $\gamma = 81{\cdot}73\ (1)$°, $V = 861{\cdot}5$ Å^3, $Z = 1$, $T = 296$ K, $D_m = 1{\cdot}05$, $D_x = 1{\cdot}05$ g cm^{-3}, $F(000) = 304$, Mo $K\alpha$, $\lambda = 0{\cdot}7107$ Å, $\mu = 0{\cdot}723$ cm^{-1}, $R = 0{\cdot}062$ for 2198 independent reflections with $I > \sigma(I)$. (II) Piperazinium *n*-hexadecanoate (palmitate), $C_4H_{12}N_2^{2+}.2C_{16}H_{31}O_2^-$, $M_r = 598{\cdot}95$, m.p. = 370·2 K, triclinic, $P\bar{1}$, $a = 5{\cdot}678\ (1)$, $b = 7{\cdot}472\ (1)$, $c = 22{\cdot}916\ (3)$ Å, $\alpha = 84{\cdot}64\ (1)$, $\beta = 89{\cdot}82\ (1)$, $\gamma = 81{\cdot}32\ (1)$°, $V = 956{\cdot}8$ Å^3, $Z = 1$, $T = 296$ K, $D_m = 1{\cdot}04$, $D_x = 1{\cdot}04$ g cm^{-3}, $F(000) = 336$, Mo $K\alpha$, $\lambda = 0{\cdot}7107$ Å, $\mu = 0{\cdot}708$ cm^{-1}, $R = 0{\cdot}052$ for 1931 independent reflections with $I > \sigma(I)$. These crystal structures, together with the previously reported *n*-decanoate and *n*-dodecanoate (laurate) salts, form an isostructural series. The piperazinium cations, which have a crystallographic centre of symmetry, are in

0108-7681/91/060968-08$03.00